Mon. Not. R. Astron. Soc. **358,** 105–112 (2005) doi:10.1111/j.1365-2966.2005.08736.x

Carbon monoxide in low-mass dwarf stars

Hugh R. A. Jones,[1,2]★ Yakiv Pavlenko,[3] Serena Viti,[4] R. J. Barber,[4]
Larisa A. Yakovina,[3] David Pinfield[1] and Jonathan Tennyson[4]

[1]*Centre for Astrophysics Research, University of Hertfordshire, College Lane, Hatfield, Hertfordshire AL10 9AB*
[2]*Astrophysics Research Institute, Liverpool John Moores University, Twelve Quays House, Egerton Wharf, Birkenhead CH41 1LD*
[3]*Main Astronomical Observatory of Academy of Sciences of Ukraine, Golosiiv woods, Kyiv-127, Ukraine 03680*
[4]*Department of Physics and Astronomy, University College London, Gower Street, London WC1E 6BT*

Accepted 2004 December 10. Received 2004 December 6; in original form 2004 July 23

ABSTRACT

We compare high-resolution infrared observations of the CO 2–0 bands in the 2.297–2.310 μm region of M dwarfs and one L dwarf with theoretical expectations. We find a good match between the observational and synthetic spectra throughout the 2000–3500 K temperature regime investigated. None the less, for the 2500–3500 K temperature range, the temperatures that we derive from synthetic spectral fits are higher than expected from more empirical methods by several hundred kelvin. In order to reconcile our findings with the empirical temperature scale, it is necessary to invoke warming of the model atmosphere used to construct the synthetic spectra. We consider that the most likely reason for the back-warming is missing high-temperature opacity due to water vapour. We compare the water vapour opacity of the Partridge–Schwenke line list used for the model atmosphere with the output from a preliminary calculation by Barber & Tennyson. While the Partridge–Schwenke line list is a reasonable spectroscopic match for the new line list at 2000 K, by 4000 K it is missing around 25 per cent of the water vapour opacity. We thus consider that the offset between empirical and synthetic temperature scales is explained by the lack of hot water vapour used for computation of the synthetic spectra. For our coolest objects with temperatures below 2500 K, we find best fits when using synthetic spectra which include dust emission. Our spectra also allow us to constrain the rotational velocities of our sources, and these velocities are consistent with the broad trend of rotational velocities increasing from M to L.

Key words: stars: atmospheres – stars: fundamental parameters – stars: late-type – stars: low-mass, brown dwarfs – stars: Population II – infrared: stars.

1 INTRODUCTION

Low-mass dwarf stars dominate our Galaxy in terms of number. They provide a probe of our understanding of main-sequence stellar evolution and are the key in determining the boundary between stellar and substellar objects. There are relatively few observations of known-mass low-mass stars. Parameters such as effective temperature and metallicity, vital in determining positions in Hertzsprung-Russell (HR) diagrams, remain controversial. To reliably constrain the low-mass initial stellar mass function, it is essential to know the basic properties of standard low-mass M, L and T dwarfs. A correct determination of the mass function relies on an accurate transformation from luminosity and temperature to mass. These relationships are sensitive to the stellar chemical composition. For hotter objects, colour–colour diagrams are reasonably reliable indicators of temperature and metallicity. However, such diagrams for low-mass dwarfs do not yet reproduce the broad-band fluxes within a reasonable error, and therefore cannot be uniquely used to determine reliable temperatures, metallicities and gravities. Ideally, it would be useful to have spectroscopic signatures sensitive to temperature, metallicity and gravity that are reproducible with synthetic spectra.

Many authors have determined the properties of low-mass objects using synthetic spectra. However, the use of such synthetic spectra are problematic because (i) the objects are dominated by various diatomic and triatomic molecules whose high-temperature properties are poorly understood and (ii) the large number of different transitions means that most transitions are substantially blended with other competing opacities. One potential route to resolve these issues is to try to find spectral regions where these issues are less problematic. For example, the middle of the *J*-band window is a promising region (Jones et al. 1996; McLean et al. 2003). Although this region is relatively transparent and is in a wavelength regime where infrared spectrometers are relatively sensitive, it does have

★E-mail: hraj@star.herts.ac.uk

shortcomings. In addition to the problems with modelling water vapour at short wavelengths (Jones et al. 2002), it is now clear that the poorly modelled opacities of FeH (Cushing et al. 2003), as well as VO and TiO (McGovern et al. 2004), also play an important role in this region.

Here we investigate an alternative wavelength regime. In the spectral region between 2.29 and 2.45 μm, CO is a key opacity for low-mass stars. CO appears in a relatively easily observed stable part of the *K* band, and molecular data, including *f* values, are well known. Moreover, CO is believed to be formed under local thermodynamic equilibrium (LTE; e.g. Carbon, Milkey & Heasley 1976) and therefore the levels are populated according to the Boltzmann distribution. The available CO line list has proven to be reliable for solar work and so is believed to be more than adequate for the lower-energy states accessed in cool dwarf atmospheres (Goorvitch 1994). The other significant metal diatomic species appearing in infrared cool dwarf stars are FeH, VO and TiO; however, these diatomics are not as prominent as CO at wavelengths obtainable with the infrared echelle used for these observations.

In Pavlenko & Jones (2002) we showed that the $\Delta v = 2$ carbon monoxide bands around 2.3–2.4 μm can be well modelled by synthetic spectra. This region is dominated by CO and H_2O bands, and has few atomic lines of significance. This is advantageous because CO is well modelled relative to the current quality of atomic oscillator strengths in the infrared (e.g. Jones et al. 1996; Lyubchik et al. 2004). Here we extend this work to much higher resolution, where the CO bands are very distinct from the water vapour modelled continuum. The wavelength range (2.297–2.311 μm) was chosen on the basis of features in late-type dwarf spectra identified to be relatively metallicity sensitive and reproducible by synthetic spectra in Viti et al. (2002).

2 OBSERVATIONS

The targets chosen for this study are all bright, relatively well-studied M and L dwarfs. The source selection was made in order to give good coverage in spectral type and metallicity. However, the half nights available to us limited our sample to a relatively restricted range of right ascension. The sample is shown in Table 1.

The targets were observed during the first half of the nights of 2001 September 8–12 with the Cooled Grating Spectrometer 4 (CGS4) on the UK Infrared Telescope (UKIRT) on Mauna Kea, Hawaii. The weather was photometric throughout with optical seeing of typically 0.8 arcsec. Comparison sky spectra were obtained by nodding the telescope so that the object was measured successively in two rows of the array, separated by 30 arcsec.

The echelle grating in 24th order at a central wavelength setting of 2.304 μm was used for all observations. This set-up gives wavelength coverage from 2.297 to 2.311 μm at a resolution of approximately 42 000.

To remove telluric bands of water, oxygen, carbon dioxide and methane, we observed A and B standard stars. Such stars are not expected to have features in common with cool dwarf stars and appear to be featureless across our spectral range. Wavelength calibration was carried out using a xenon arc lamp. This generally worked well because, although there are only four lines available in this region, the xenon lines at 2.29 and 2.31 μm fall at either edge of the array and so provide a good wavelength calibration. The only caveat to this is that the wavelength positioning of the echelle is only accurate to around 20 pixels and so the desired wavelength interval is sometimes shifted redward or blueward by around 0.001 μm. Our cross-correlation tests indicate that the wavelength calibration was better than 0.0001 μm. Sky subtraction was carried out with standard routines, which take into account any residual sky emission due to variation of the sky brightness between paired object and sky spectra. The signal was spread between three rows. To extract the spectrum from the sky-subtracted signal, an optimal extraction technique was used; this combines the rows using weights based on the spatial profile of the stellar image. The spectra were reduced using the FIGARO, SPECDRE and KAPPA packages provided and supported by Starlink.

Table 1. Literature properties of observed targets: kinematic classification (KIN-class) are from Leggett (1992) and Leggett, Allard & Hauschildt (1998), spectral types are from Kirkpatrick, Henry & McCarthy (1991) and Gizis (2002), and empirical temperatures are derived using Lane et al. (2001), Segransan et al. (2003), Dahn et al. (2002) and Vrba et al. (2004).

Object	KIN-class	Sp type	Empirical temperature (K)
GJ860A	OD	dM3	3310
GJ725A	OD	dM3	3310
GJ725B	OD	dM3.5	3230
GJ896A	YD	dM3.5	3230
G87−9B	–	dM4	3150
GJ699	O/H	dM4	3150
GJ860B	OD	dM4	3150
GJ896B	YD	dM4.5	3070
GJ630.1A	H	dM4.5	3070
GJ166C	OD	dM4.5	3070
GJ2005ABCD	OD	dM5.5	2910
GJ65A	YD	dM5.5	2910
GJ65B	YD	dM6	2825
GJ644C	OD	dM7	2670
GJ752B	OD	dM8	2550
LP944−20	YD	dM9	2440
2MASS0036	–	dL4	1900

A spectral sequence from M3 to L4 is shown in Fig. 1. It can be seen from Fig. 2 that individual rotational CO transitions can be resolved in our observed spectra. The CO opacities in our spectra are made up of a large number of spectral lines, covering a wide intensity range, of the second overtone ($\nu = 2$–0). The second overtone band of CO originates from vibration–rotation transitions in the ground electronic state $X^1\Sigma$ and obeys the selection rules $\Delta v = 2$ and $\Delta J = \pm 1$. The band head of the second overtone (i.e. the point at which the separation between the R transitions is zero)

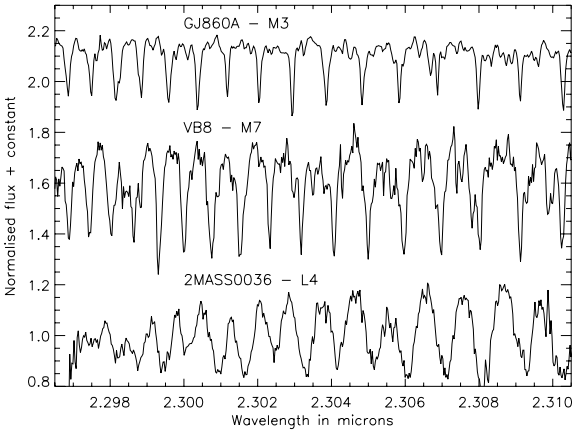

Figure 1. Spectral sequence of CO bands from M3 to L4.

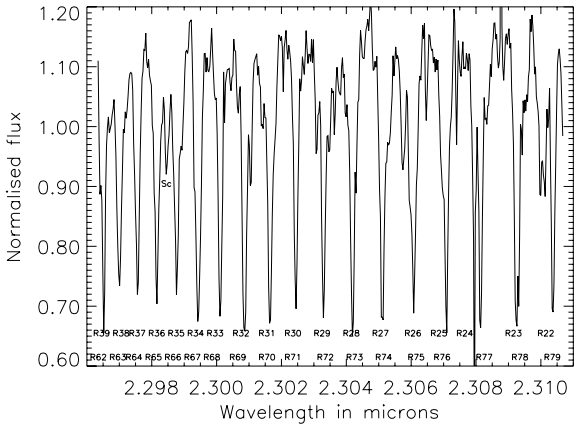

Figure 2. CO 2–0 transitions and Sc line identified in GJ752B. The resolution of the data is insufficient to unambiguously identify the higher energy (R62 to R79). The R24 and R77 transitions appear to be resolved from one another; however, inspection of Fig. 3 indicates that the left-hand feature is due to water vapour.

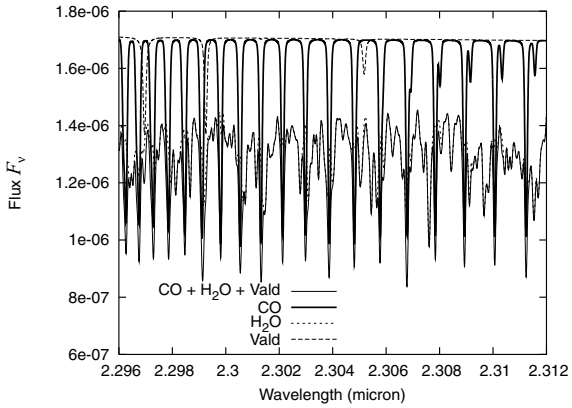

Figure 3. The plot shows the various opacity contributions for a 3000 K, $\log g = 5.0$ solar metallicity model from atomic lines (top of plot, dashed line), carbon monoxide transitions (top of the plot, thick solid line), water vapour (dotted line) and the overall formation of the continuum primarily dominated by water (thin solid line).

occurs at ∼2.290 μm and therefore both 'hot' (such as R77) and 'cold' (such as R24) rotational transitions are seen in our spectra.

3 THE MODELS

Model atmospheres from the Phoenix code were used for this work. In particular, we used the grid known as NextGen (Hauschildt, Allard & Baron 1999), but also Dusty (Allard et al. 2001) and AMES-COND models (Allard et al. 2001). Model temperatures of 1500–3800 K, metallicities of [M/H] = −2.0–0.0 and gravities of $\log g = 4.5$–5.5 are considered. These parameters represent the probable extremes for the sample based on the literature. We have not tried comparing the system with models computed with non-solar abundance patterns.

Computations of local thermal equilibrium synthetic spectra were carried out by the program WITA6 (Pavlenko 2000). This model assumes LTE, hydrostatic equilibrium for a one-dimensional model atmosphere, and no sources or sinks of energy. The equations of ionization–dissociation equilibrium were solved for media consisting of atoms, ions and molecules. We took into account ∼100 components (Pavlenko 2000). The constants for equations of chemical balance were taken from Tsuji (1973). It is worth noting that the chemical balance in cool dwarf atmospheres is governed by the CO molecule (Pavlenko & Jones 2002).

The Partridge & Schwenke (1997, hereafter PS) line list is used as the primary source of water vapour lines, although we also made some comparisons with the preliminary line list of Barber and Tennyson (in preparation, hereafter BT1). The partition functions of H_2O were also computed on the PS line list following Pavlenko et al. (2004). We recomputed the constants of dissociation equilibrium using the H_2O partition function following Vidler & Tennyson (2000), although we found no significant differences for test synthetic spectra at 3200 K, $\log g = 5$ and 2400 K, $\log g = 5$ (Pavlenko et al., in preparation). For CO, we used the $^{12}C^{16}O$ and $^{13}C^{16}O$ line lists of Goorvitch (1994). The CO partition functions were taken from Gurvitz, Weitz & Medvedev (1982). The atomic line list was taken from the Vienna Atomic Line Data base (VALD; Kupka et al. 1999). The relative importance of the different opacities contributing to our synthetic spectra is shown in Fig. 3.

The profiles of molecular and atomic lines are determined using the Voigt function $H(a, v)$, parameters of their natural broadening C_2 and van der Waals broadening C_4 from data bases (Kupka et al. 1999) or in their absence computed following Unsold (1955). Owing to the low temperatures in cool dwarf atmospheres, and consequent low electron densities, Stark broadening may be neglected. Computations for synthetic spectra were carried out with a 0.00005-μm step for microturbulent velocities $v_t = 1$, 2 and 3 km s^{-1}. The sensitivity of the spectral region to changes in model parameters is shown in Fig. 4. It can be seen that temperature has a relatively larger effect on the depth of the CO features than metallicity and gravity. In this regard, a temperature change of 200 K is roughly equivalent to a change in metallicity of 1 dex or a change in gravity of $\Delta\log g = 1$.

The instrumental broadening was modelled by triangular profiles set to the resolution of the observed spectra. To find the best fits to observed spectra, we follow the scheme of Jones et al. (2002). Namely, for every spectrum we carry out the minimization of a three-dimensional function $S = f(x_s, x_f, x_w) = 1/N \times \sum(1 - F_{obs}/F_{synt})^2$, where F_{obs} and F_{synt} are observed and computed fluxes, N is the number of points in the observed spectrum to be fitted, and x_s, x_f and x_w are relative shifts in wavelength scale, flux normalization factor and instrumental + rotational broadening, respectively. Rotational broadening was computed following Gray (1992). Fig. 5 shows the sensitivity of our fit for GJ752B to the various model parameters. Fig. 6 shows the observed and synthetic spectra fit for each object.

4 SPECTROSCOPIC ANALYSIS

The effective temperatures given in Table 1 were derived by averaging the temperatures derived by Dahn et al. (2002) and Vrba et al. (2004) across each spectral type and neglecting very young objects from the determination. For example, a much lower effective temperature is derived for LP944−21; however, there is strong evidence (e.g. Ribas 2003) that the age of this object is <0.5 Gyr rather than the 3 Gyr assumed by the methodology of Dahn et al. (2002) and Vrba et al. (2004). For early spectral types, we use the effective temperature scales derived from Lane et al. (2001) and Segransan et al. (2003). We note these are consistent with detailed studies of GJ630.1A (Viti et al. 2002) and GJ699 (Dawson & de Robertis 2004). From here on, we consider the effective temperatures in

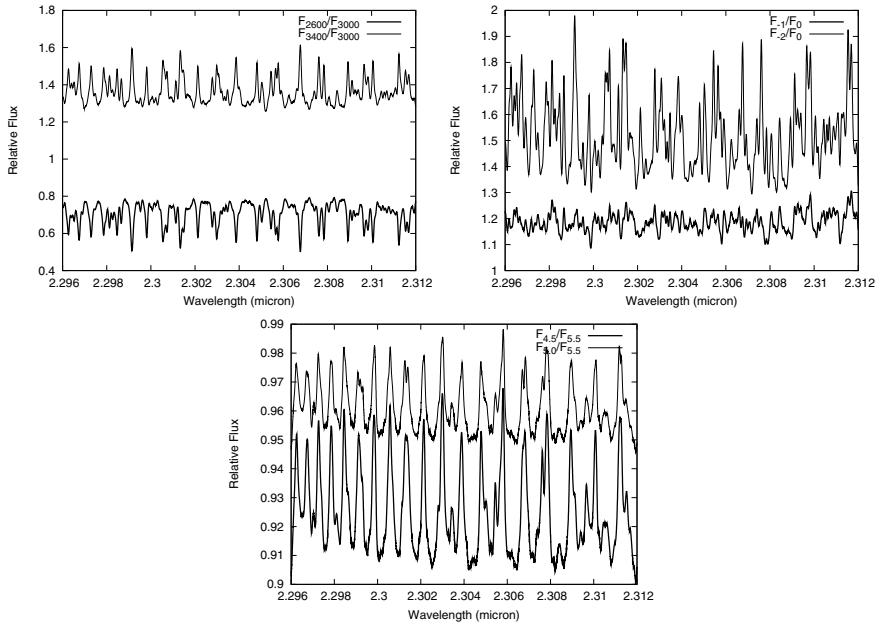

Figure 4. The plots show the temperature (top-left), metallicity (top-right) and gravity (bottom) dependence of synthetic spectra around a base model of 3000 K, solar metallicity, $\log g = 5.0$. The value of the model atmosphere parameter being adjusted is indicated as subscript. For example, in the top-right plot, the label F_{-1}/F_0 indicates the flux (F) of a 3000 K, [M/H] $= -1$, $\log g = 5.0$ model divided by a 3000 K, [M/H] $= 0$, $\log g = 5.0$ model.

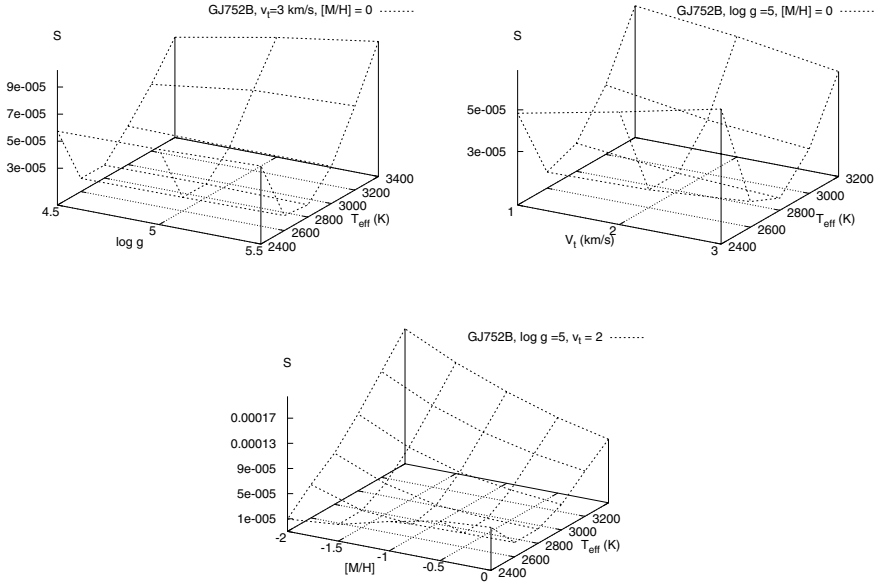

Figure 5. Surface plots showing the sensitivity of the best-fitting temperature of GJ752B to metallicity, gravity and turbulent velocity. A base model of solar metallicity, $\log g = 5.0$ and $v_t = 3$ km s^{-1} is used.

Table 1 as 'empirical', although this does assume that the radii of the evolutionary models that were used are accurate. Based on the comparisons of Chabrier & Baraffe (1995), this seems a reasonable working assumption.

In Table 2, we present best-fitting parameters determined using our minimization technique on our observational spectra of sources with spectral types $\leqslant$M8. As suggested by the work of Mohanty & Basri (2003) and Bailer-Jones (2004), it appears that our rotational velocities show a general increase toward later spectral types. However, with the modest sample size presented here, we are not in a position to further advance this area of work. None the less, it should be noted that the density of strong CO features makes this an efficient region in which to derive rotational velocities and radial velocities. In addition to so-called 'unconstrained fits' where minimization takes into account all parameters, we also give two cases of 'constrained fits'. In the first constrained fit, we set [M/H] $= 0$ and fit $T_{\rm eff}$ and $\log g$, and in the second constrained fit we set $T_{\rm eff}$ equal to the empirical $T_{\rm eff}$ and fit $\log g$ and [M/H].

Our unconstrained minimization solutions suggest temperatures higher than would be expected from the empirical temperatures of the objects. Relatively high temperatures are also found for the [M/H] $= 0$ constrained fit. Our empirical $T_{\rm eff}$ constrained fit

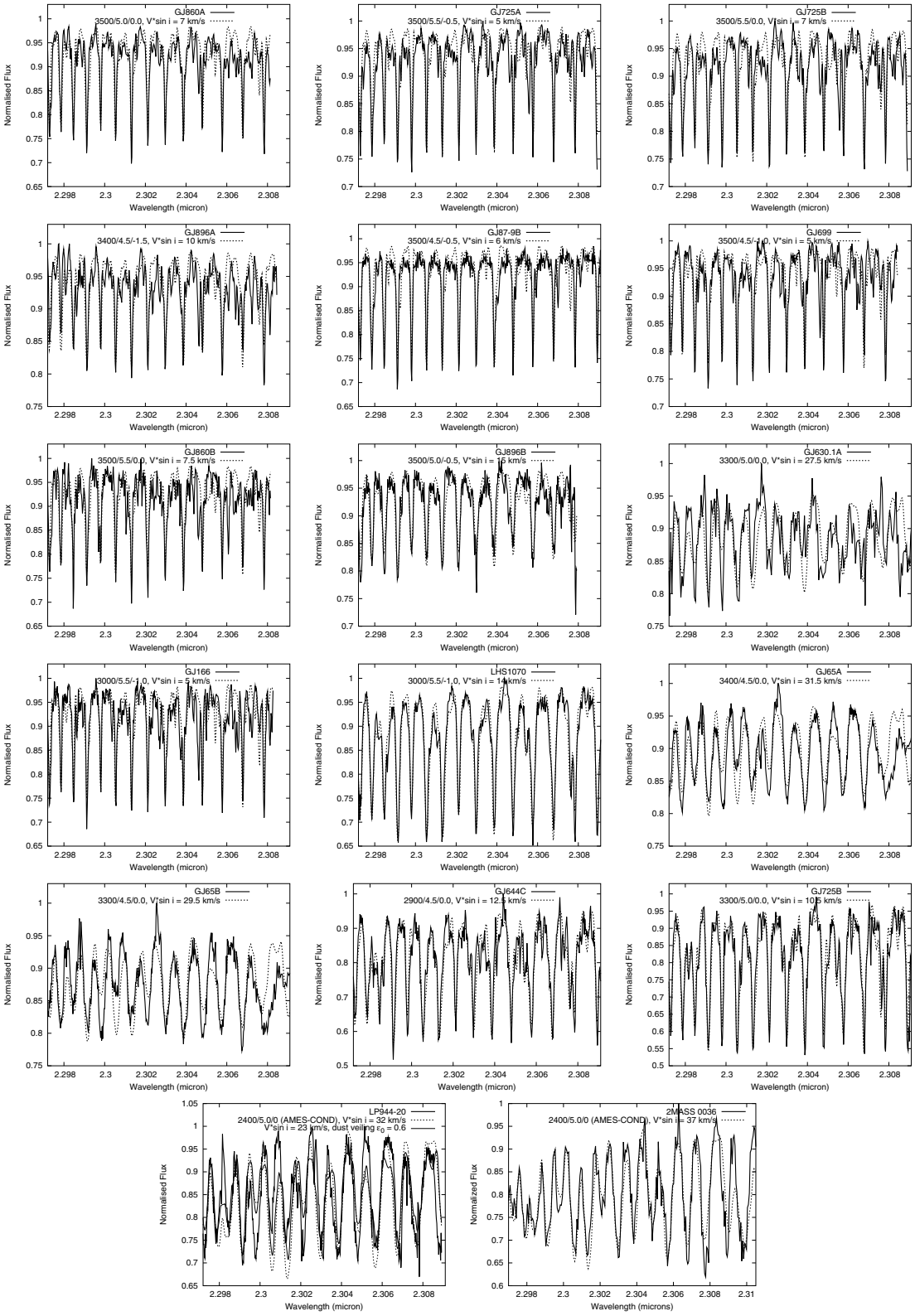

Figure 6. The observational data are overlaid with the best-fitting 'unconstrained' synthetic spectra except for LP944−20 and 2MASS0036 for which representative models are shown.

indicates a tendency to improbably low metallicities for almost all of the sample. We consider this discrepancy to arise from the fact that CO bands become weaker for decreasing metallicity or increasing temperature in a similar manner. Thus, if the models want to fit a higher $T_{\rm eff}$, but are forced to fit a lower one, then they will fit a lower [M/H] to compensate.

In Fig. 7 we plot empirical and derived temperature scales against one another. It can be seen that for almost all objects our 'derived'

Table 2. Derived synthetic spectra parameters are given. The syntax for the models is $T_{\rm eff}/\log g/[{\rm M/H}]$; so, for example, 2800/5.0/−0.5 means a 2800 K, gravity = 5.0 cm s^{-1} and metallicity −0.5 dex model. Rotational velocities are derived from the unconstrained minimization fit and are typically accurate to 3 km s^{-1}. Values given in italic are fixed. The values for the minimization of coolest objects LP944−20 and 2MASS0036 (shortened version of its full designation of 2MASS J00361617+1821104) are rather dependent on the details of the model. Minimizations for these objects are presented in Fig. 9.

Object	Rotational velocity $v \sin i$ (km s^{-1})	Unconstrained minimization	[M/H] constrained $T_{\rm eff}$ and log g minimization	$T_{\rm eff}$ constrained [M/H] and log g minimization
GJ860A	7.0	3500/5.5/0.0	3500/5.5/*0.0*	*3300*/5.0/−1.0
GJ725A	5.0	3500/5.5/−0.5	3600/5.5/*0.0*	*3300*/5.0/−1.5
GJ725B	7.0	3500/5.5/0.0	3500/5.5/*0.0*	*3200*/5.0/−1.5
GJ896A	10.0	3400/4.5/−1.5	3600/5.5/*0.0*	*3200*/4.5/−2.0
G87−9B	6.0	3500/4.5/−0.5	3500/5.5/*0.0*	*3200*/5.0/−1.5
GJ699	5.0	3500/4.5/−0.5	3600/5.5/*0.0*	*3200*/4.5/−2.0
GJ860B	8.0	3500/5.5/0.0	3500/5.5/*0.0*	*3200*/4.5/−1.5
GJ896B	15.0	3500/5.0/−0.5	3500/5.5/*0.0*	*3100*/4.5/−2.0
GJ630.1A	27.5	3300/5.0/−0.5	3300/5.0/*0.0*	*3100*/4.5/0.0
GJ166C	5.0	3400/5.5/−0.5	3500/5.5/*0.0*	*3000*/4.5/−2.0
GJ2005ABCD	14.0	3000/5.5/−1.0	3300/4.5/*0.0*	*2900*/5.0/−1.5
GJ65A	31.5	3400/4.5/0.0	3400/4.5/*0.0*	*2900*/5.5/−1.5
GJ65B	29.5	3300/4.5/0.0	3300/4.5/*0.0*	*2800*/5.5/−1.5
GJ644C	12.5	2900/4.5/0.0	2900/4.5/*0.0*	*2700*/5.0/−1.0
GJ752B	10.5	2900/5.5/0.0	2900/5.5/*0.0*	*2600*/5.0/−1.5
LP944−30	31.0	–	–	–
2MASS0036	38.0	–	–	–

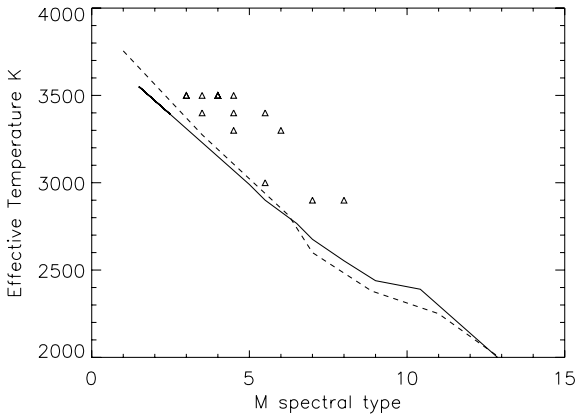

Figure 7. The triangles indicate best-fitting temperatures for the observed sample given synthetic spectra where the metallicities are constrained to be solar and gravities constrained to be $\log g = 5.0$. The solid line shows our adopted 'empirical' temperature scale, and the dashed line shows a recent alternative scale from Golimowski et al. (2004).

effective temperatures (triangles) are higher than expected for empirical temperatures. Given the good match of synthetic to observed spectral features, one might expect more similar empirical and synthetic temperature scales. Such a discrepancy between empirical and synthetic temperature scale is a long-standing result, which has been arrived at by a number of routes: from fits to (i) the overall spectral energy distribution (e.g. Berriman & Reid 1987), (ii) atomic lines (e.g. Jones et al. 1996), (iii) water vapour (Jones et al. 2002) and (iv) carbon monoxide (e.g. Pavlenko & Jones 2002). However, the temperature discrepancy for low-mass stars is usually discussed for stars with $T_{\rm eff} < 3000$ K, and is generally taken to be an effect arising from the inability of models to accurately treat dust formation (e.g. Dahn et al. 2002). We find the temperature discrepancy for apparently well-modelled spectra to be prevalent up to at least 3500 K. On the premise that the 'empirical' temperature scales are closer to reality, the offset suggests that the model structures are too hot for a given effective temperature. For GJ752B, we have experimented with altering the model temperature structure. We find that substantial structural changes are necessary to adjust synthetic temperatures by the few hundred kelvin needed to fit empirical ones. Because temperature discrepancies of 200 K translate into uncertainties of 1 dex in [M/H] or $\Delta \log g = 1$ it is not possible to have confidence in our minimization values for these properties. The temperature offset for the cooler objects such as GJ752B ($T_{\rm eff} = 2550$ K) might be explained by the presence of relatively poorly quantified dust opacities. However, because the offset is also apparent above 3000 K where dust will not form (e.g. Tsuji 2002) it seems likely that at least part of the temperature scale problem is not due to dust. Instead we consider that the temperature scale problem may arise from a lack of high-temperature water opacities.

As expected from our previous high-resolution CO work (Viti et al. 2002), our current fits of the synthetic to observational spectra are encouraging. This is primarily due to our choice of a spectral region dominated by a well-understood absorber (CO). However, it is clear from Fig. 3 that water vapour opacity also plays a role in this spectral region. While the PS water vapour line list is clearly excellent at long wavelengths (Jones et al. 2002), there are significant discrepancies around 1.6 and 2.2 μm (Allard, Hauschildt & Schwenke 2000) and most probably around 0.95 μm as well.

In Fig. 8 we compare the PS water vapour line lists with the preliminary line list of BT1. The current version of the BT1 list is fully converged and complete to $J = 50$ and includes around 650 million transitions. The PS list is also complete in respect to J levels (it reaches $J = 55$) and consists of around 308 million transitions. The PS list is cut off at approximately 28 000 cm^{-1} (approximately, as there is not a consistent cut-off level), whereas the BT1 list has a cut-off of 30 000 cm^{-1}. Moreover, even at energies below 28 000 cm^{-1} many lines are missing in the PS list (probably due to lack of convergence, resulting in the omission of higher levels). The BT1 list uses a newer potential surface (Shirin et al. 2003) and better describes high-temperature water vapour transitions. Fig. 8 indicates that at 2000 K the line lists give rather similar results, although by 4000 K BT1 shows approximately a 25 per cent increase in

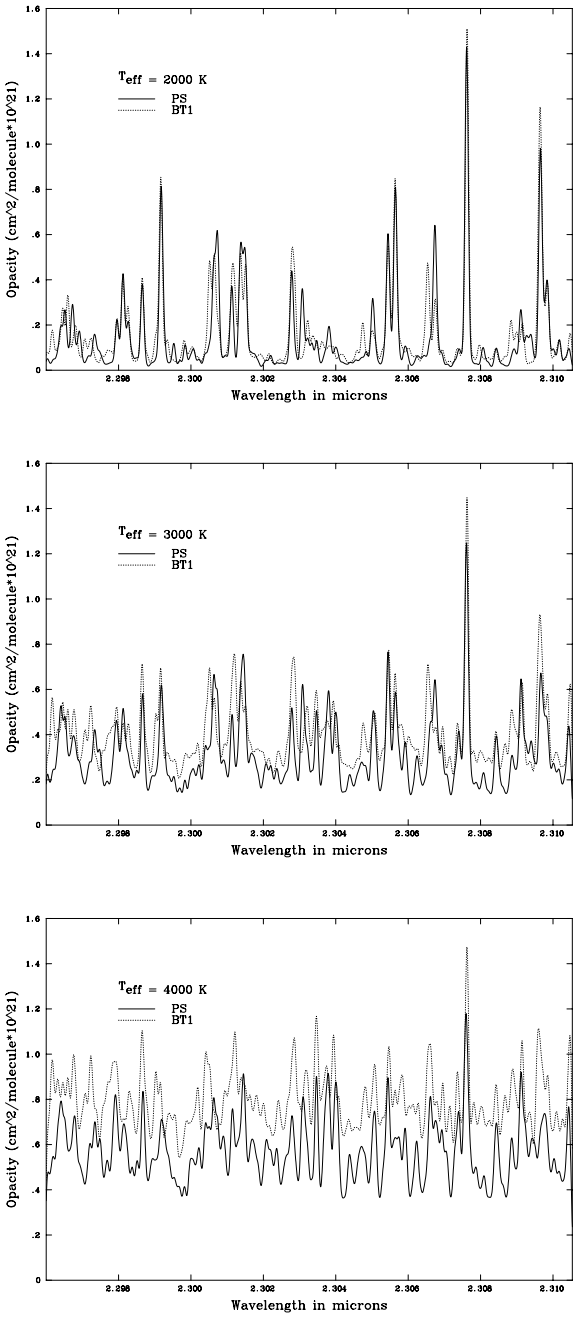

Figure 8. Water vapour opacity for different water vapour line lists: the solid line shows the PS list and the dotted line the BT1 list. While across the chosen wavelength region they are spectroscopically similar, the overall opacity is rather different.

opacity. Spectroscopically, the line lists are reasonably similar although substantial differences can be seen by 4000 K. It is clear that the extra opacity of BT1, arising from higher J levels and improved completeness, will lead to a significant back-warming effect on the model atmosphere, moving the photosphere outward and the effective temperature downward. We checked for spectral differences between BT1 and PS; however, they are relatively small and make no difference to our derived minimization values. To see the effect of the increased opacity on the atmospheric structure of cool dwarfs, it will be necessary to compute a new grid of model atmospheres. This will begin once the process of checking the BT1 list is complete, for example, by assigning quantum numbers to the transitions of lines in the laboratory emission spectrum of water at 3200 K (Coheur et al. 2005).

4.1 Below 2500 K: LP944 and 2MASS0036

Below 2500 K we do not easily find a satisfactory minimization solution for the M9 dwarf LP944−20 and the L4 dwarf 2MASS0036, using any of the grids of model atmospheres (NextGen, AMES-Cond and Dusty). The results of our experiments are shown in Fig. 9. The dusty and non-dusty models (solid and short-dashed lines, respectively) both suggest best-fitting temperatures higher than the edge of the model grid (>2600 K). While such temperatures might possibly be plausible for LP944−20, the 'empirical' temperature for 2MASS0036 is a mere 1900 K. While incomplete water vapour may be crucial at higher temperature, the relative similarity of the PS and BT1 line lists around 2000 K means that water vapour opacity is unlikely to be the source of this discrepancy. The discrepancy is probably more likely to arise from an inappropriate treatment of dust opacity. While a more sophisticated dust model is certainly appropriate (e.g. Tsuji, Nakajima & Yanagisawa 2004) we also experiment with another possibility. Following the methodology of Pavlenko et al. (2004), we imagine that the 2.3-μm region is veiled by additional grey continuum absorption. The long-dashed and dotted lines in Fig. 9 indicate that veiling serves to improve the minimization values obtained and appealingly decreases the sensitivity of the model fit. While we have not considered whether the atmospheric conditions are conducive to dust emission, it is interesting that such veiling could result in spectra where CO bands do not change in strength appreciably throughout the L spectral class (Reid et al. 2001; Geballe et al. 2002; Nakajima, Tsuji & Yanagisawa 2004). Overall, the flat nature of the minimization values for 'emission on' models and minimizations beyond the model grid for 'emission off' models suggest that we are not in a position to constrain effective temperature for the coolest targets in our sample.

In order to resolve these issues, the first priority must be to incorporate a new water vapour line list in model atmosphere calculations. From an observational point of view, it is important to obtain high-resolution spectra of appropriate molecular and atomic features at widely separated wavelengths. Such observations should enable us to distinguish the importance of dust at different wavelengths. Dust absorption affects not only the synthetic spectra but the structure of the atmosphere. The problem needs to be solved with a self-consistent approach, which includes, among other things, depletion of molecular species into dust particles, the structure of dust clouds and a reliable size and composition distribution. Consideration of these issues is planned for future models and papers.

5 CONCLUSIONS

Based on a comparison of high-resolution synthetic and observed spectra in the near-infrared region, we derive rotational velocities, temperatures, metallicities and gravities for a sample of well-studied objects. While our spectra are well modelled and dominated by CO absorption bands, we find temperatures that are higher than those found by more empirical methods from 2500 to 3500 K. The discrepancy at higher temperatures is particularly interesting, and we consider it to be indicative of missing opacity, probably due to hot water vapour transitions not currently included in model atmospheres. Below $T_{\rm eff} = 2500$ K, the additional complication of dust formation is expected to be another factor that requires accurate modelling if we are to derive accurate parameters from spectral fits.

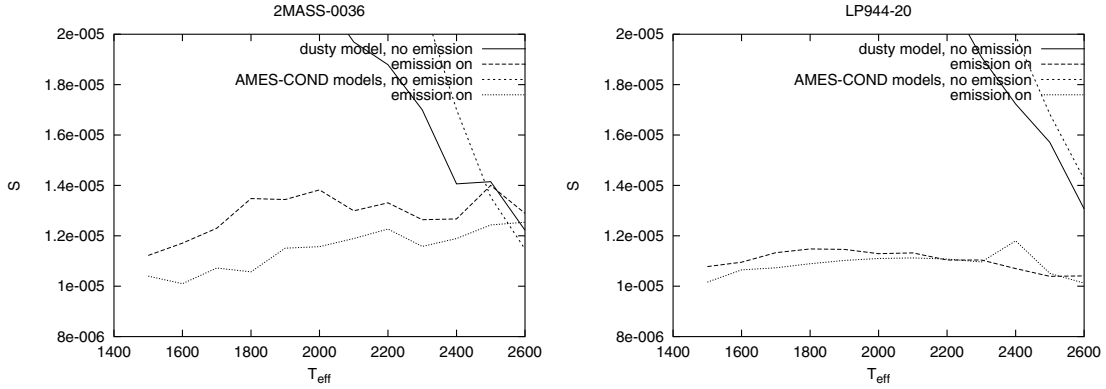

Figure 9. The minimization values for the L dwarfs 2MASS0036 and LP944 deduced using dusty and non-dusty model atmospheres with and without emission. Minimization values have been derived across the relevant model grid of temperatures although log g has been fixed at 5.0 and [M/H] has been fixed at the solar value.

ACKNOWLEDGMENTS

We thank the staff at the UKIRT for assistance with the observations, in particular Sandy Leggett. We are grateful to the UK Particle Physics and Astronomy Research Council (PPARC) and the Royal Society for travel funding. SV thanks PPARC for an advanced fellowship. We are grateful to an anonymous referee for insightful comments which improved this manuscript.

REFERENCES

Allard F., Hauschildt P. H., Schwenke D., 2000, ApJ, 540, 1005
Allard F., Hauschildt P. H., Alexander D. R., Tamanai A., Schweitzer A., 2001, ApJ, 556, 357
Bailer-Jones C. A. L., 2004, A&A, 419, 703
Berriman G., Reid N., 1987, MNRAS, 227, 315
Carbon D. F., Milkey R. W., Heasley J. N., 1976, ApJ, 207, 253
Chabrier G., Baraffe I., 1995, ApJ, 451, 29
Coheur P. F. et al., 2005, J. Chem Phys., in press
Cushing M. C., Rayner J. R., Davis S. P., Vacca W. D., 2003, ApJ, 582, 1066
Dahn et al., 2002, AJ, 124, 1170
Dawson P. C., de Robertis M. M., 2004, AJ, 127, 2909
Geballe T. R. et al., 2002, ApJ, 564, 466
Gizis J. E., 2002, ApJ, 575, 484
Golimowski D. A. et al., 2004, AJ, 127, 3516
Goorvitch D., 1994, ApJS, 95, 535
Gray D. F., 1992, The Observation and Analysis of Stellar Photospheres, 2nd edn. Cambridge Univ. Press, Cambridge
Gurvitz L. V., Weitz I. V., Medvedev V. A., 1982, Thermodynamic Properties of Individual Substances. Moscow Science, Moscow
Hauschildt P. H., Allard F., Baron E., 1999, ApJ, 512, 377
Jones H. R. A., Longmore A. J., Allard F., Hauschildt P. H., 1996, MNRAS, 280, 77
Jones H. R. A., Pavlenko Y., Viti S., Tennyson J., 2002, MNRAS, 331, 871
Kirkpatrick J. D., Henry T., McCarthy D. W., 1991, ApJS, 77, 417
Kupka F., Piskunov N., Ryabchikova T. A., Stempels H. C., Weiss W. W., 1999, A&AS, 138, 119
Lane B. F., Zapatero M. R., Britton M. C., Martin E. L., Kulkarni S. R., 2001, ApJ, 560, 390
Leggett S. K., 1992, ApJS, 82, 351
Leggett S. K., Allard F., Hauschildt P. H., 1998, ApJ, 509, 836
Lyubchik Y., Jones H. R. A., Pavlenko Y. V., Viti S., Pickering J. C., Blackwell-Whitehead R., 2004, A&A, 416, 655
McGovern M. R., Kirkpatrick J. D., McLean I. S., Burgasser A. J., Prato L., Lowrance P. J., 2004, ApJ, 600, 1020
McLean I. S., McGovern M. R., Burgasser A. J., Kirkpatrick J. D., Prato L., Kim S. S., 2003, ApJ, 596, 561
Mohanty S., Basri G., 2003, ApJ, 583, 451
Nakajima T., Tsuji T., Yanagisawa K., 2004, ApJ, 607, 499
Partridge H., Schwenke D. J., 1997, J. Chem. Phys., 106, 4618 (PS)
Pavlenko Y., 2000, Astron. Rep., 44, 219
Pavlenko Y., Jones H. R. A., 2002, A&A, 396, 967
Pavlenko Y., Geballe T. R., Evans A., Smalley B., Eyres S. P. S., Tyne V. H., Yakovina L. A., 2004, A&A, 417, L39
Reid I. N., Burgasser A. J., Cruz K. L., Kirkpatrick J. D., Gizis J. E., 2001, ApJ, 121, 1710
Ribas I., 2003, A&A, 400, 279
Segransan D., Kervella P., Forveille T., Queloz D., 2003, A&A, 397, 5
Shirin S. V., Polyansky O. L., Zobov N. F., Barletta P., Tennyson J., 2003, J. Chem. Phys., 118, 2124
Tsuji T., 1973, A&A, 23, 411
Tsuji T., 2002, ApJ, 575, 264
Tsuji T., Nakajima T., Yanagisawa K., 2004, ApJ, 607, 511
Unsold A., 1955, Physik der Sternatmospheren, 2nd edn. Springer-Verlag, Berlin
Vidler M., Tennyson J., 2000, J. Chem. Phys., 113, 9766
Viti S., Jones H. R. A., Maxted P., Tennyson J., 2002, MNRAS, 329, 290
Vrba F. J. et al., 2004, AJ, 127, 2948

This paper has been typeset from a TEX/LATEX file prepared by the author.